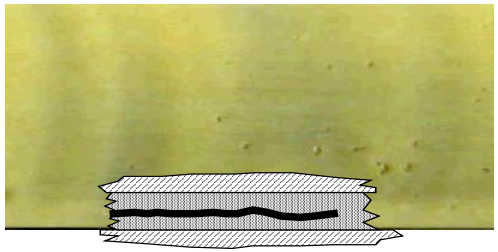

a). Cohesive Failure

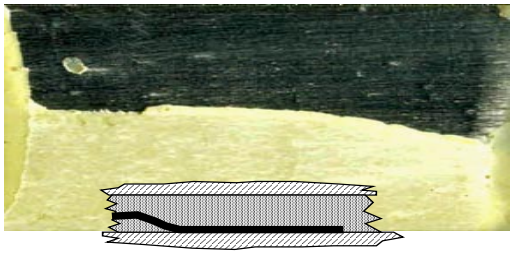

b). Interfacial Failure

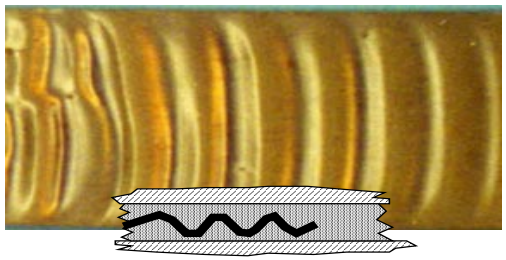

c). Oscillatory Failure

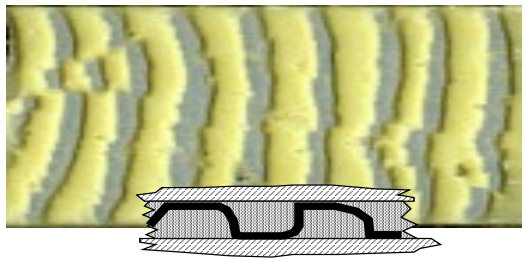

d). Alternating Failure

Fig. 1. Different locus of failure and crack trajectories observed in mode I testing of adhesively bonded double cantilever beam (DCB) specimens.

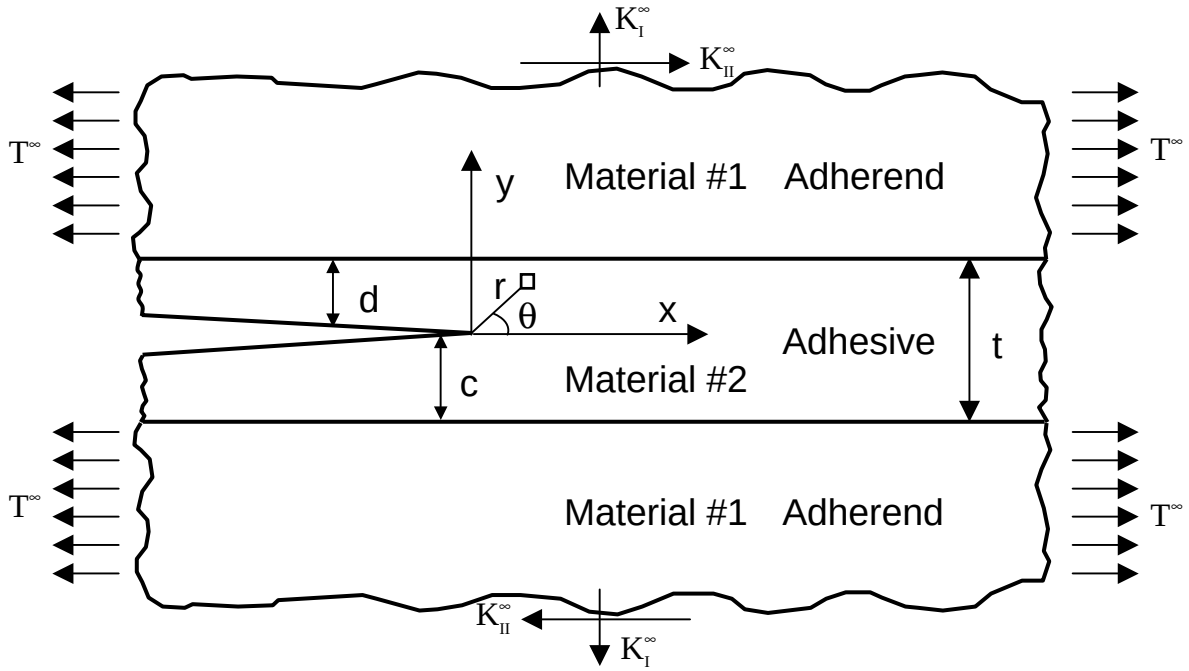

Fig. 2. A crack in an adhesive bond, the model used in the analysis by Fleck, Hutchinson, and Suo [1] and Akisanya and Fleck [4, 16]. The adherend is assumed to be semi-infinite and the bond is under a mixed mode far field loading.

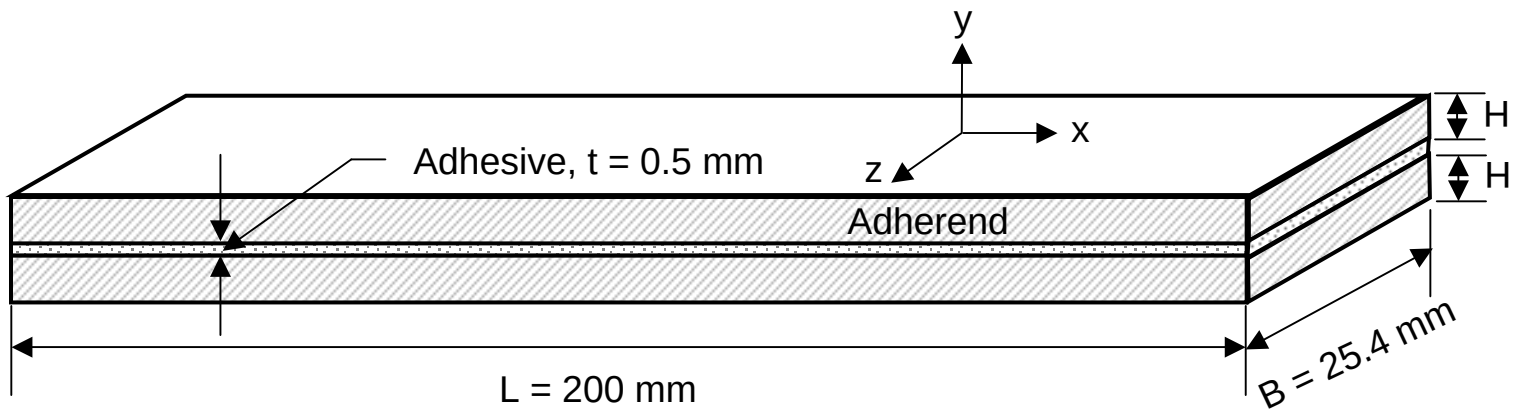

Fig. 3. Geometry of adhesively bonded double cantilever beam (DCB) specimens.

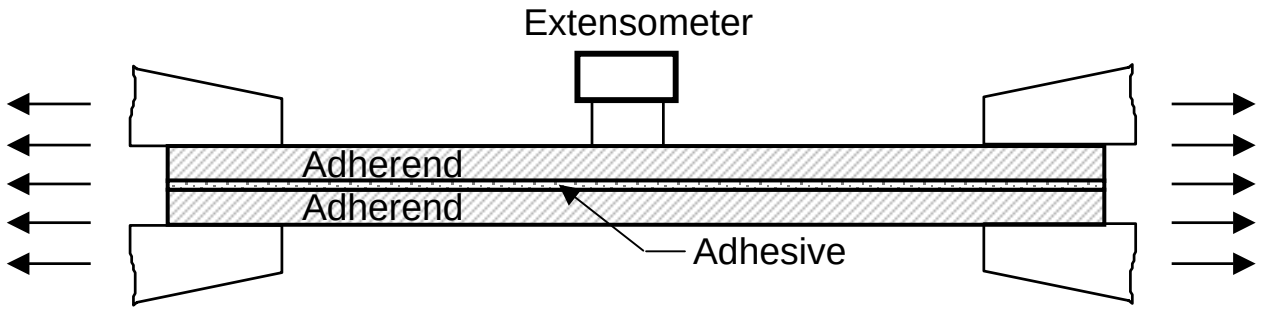

Fig. 4. Schematic of DCB specimens loaded in tension in a universal test machine until the adherends were plastically deformed in order to alter the residual stress state in the adhesive layer.

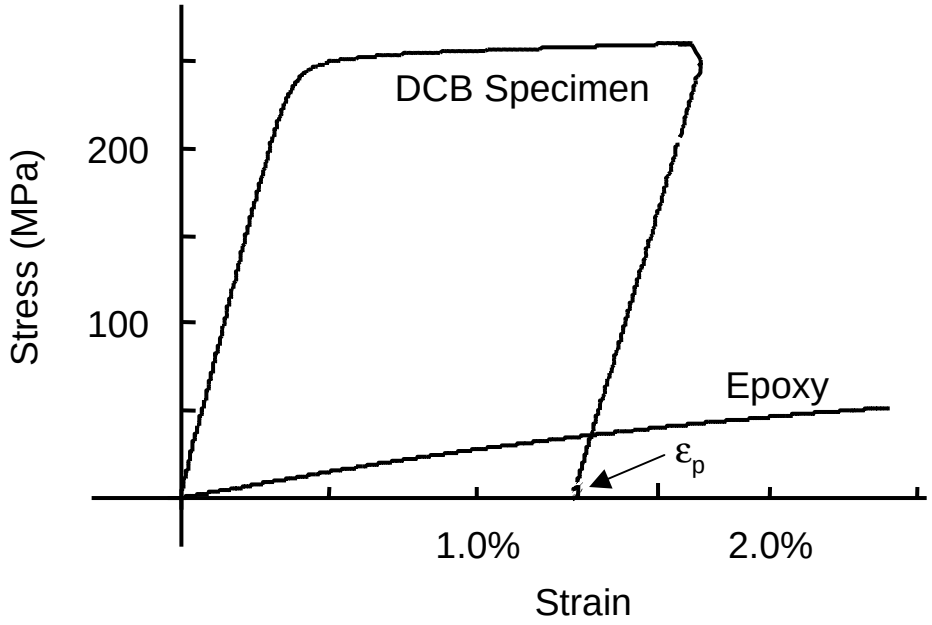

Fig. 5. The stress-strain curve for the DCB specimens under uniaxial tension and neat adhesive dogbone specimens.

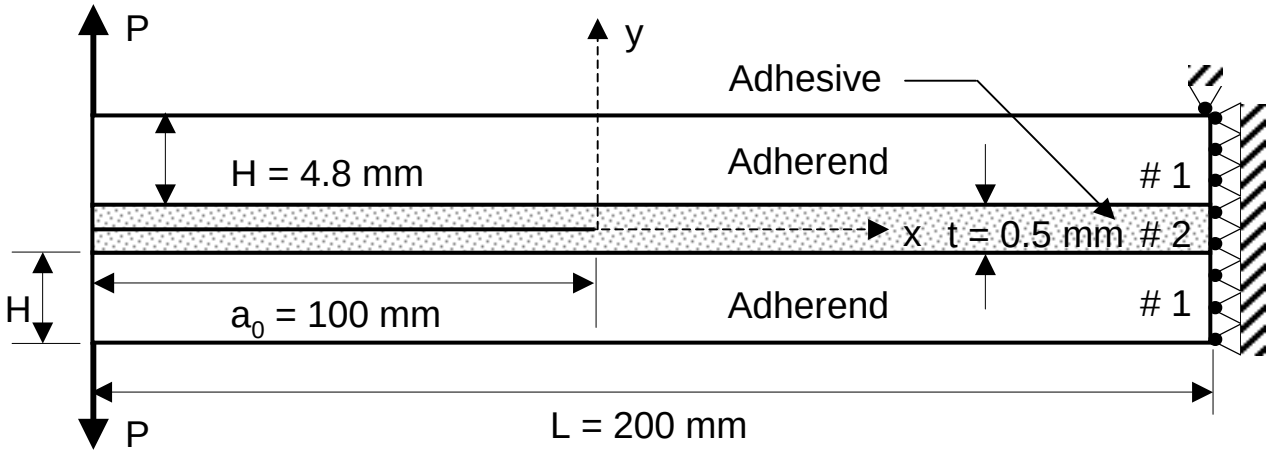

Fig. 6. The numerical DCB model used in the finite element analysis; a layer of adhesive is sandwiched between two adherends. Both adhesive and adherend are modeled as linear elastic materials with material constants E_1 = 70 GPa, E_2 = 2.97 GPa, and $\nu_1 = \nu_2 = 0.33$.

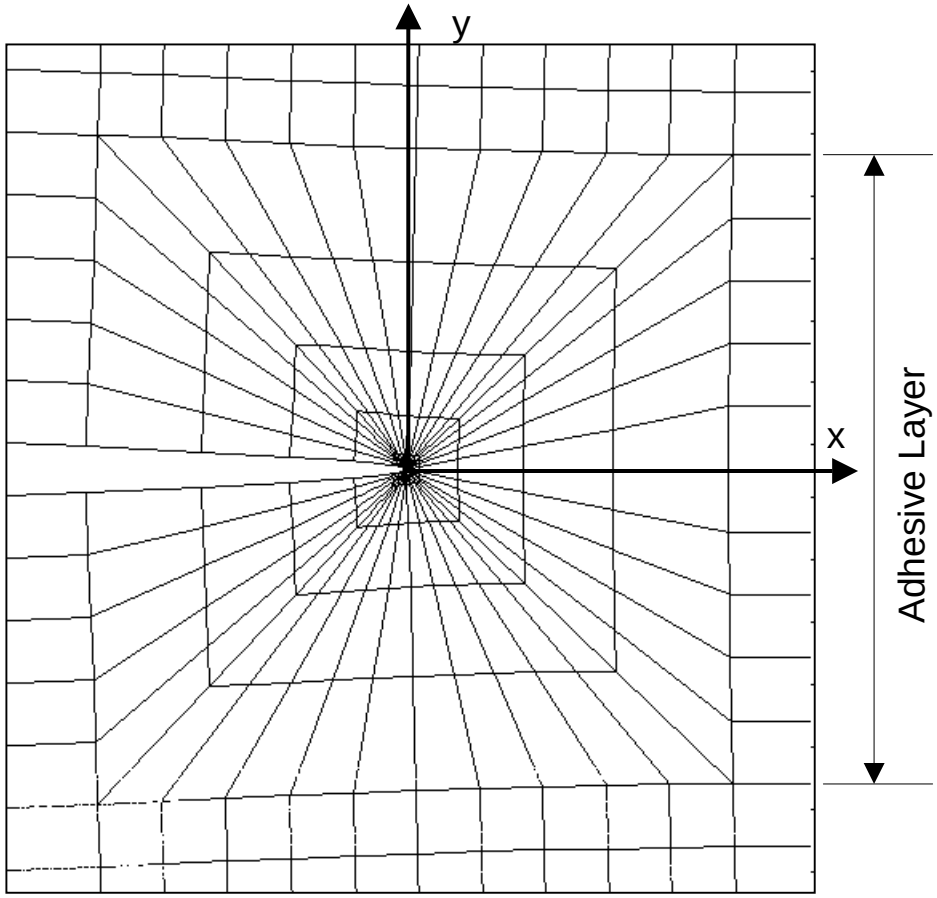

Fig. 7. The finite element mesh around the crack-tip. Eight-node, plane-strain elements were used with reduced integration and quarter point singular elements were constructed around the crack tip.

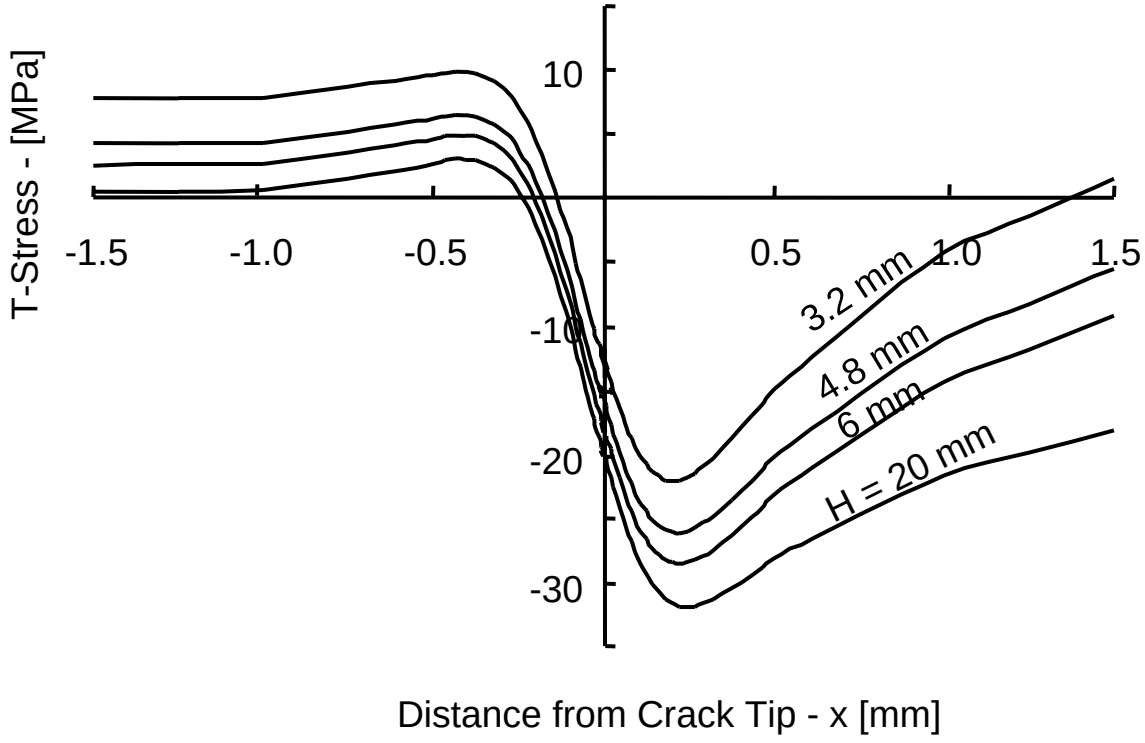

Fig. 8. The T-stresses for DCB specimens with different adherend thicknesses and zero residual stress.

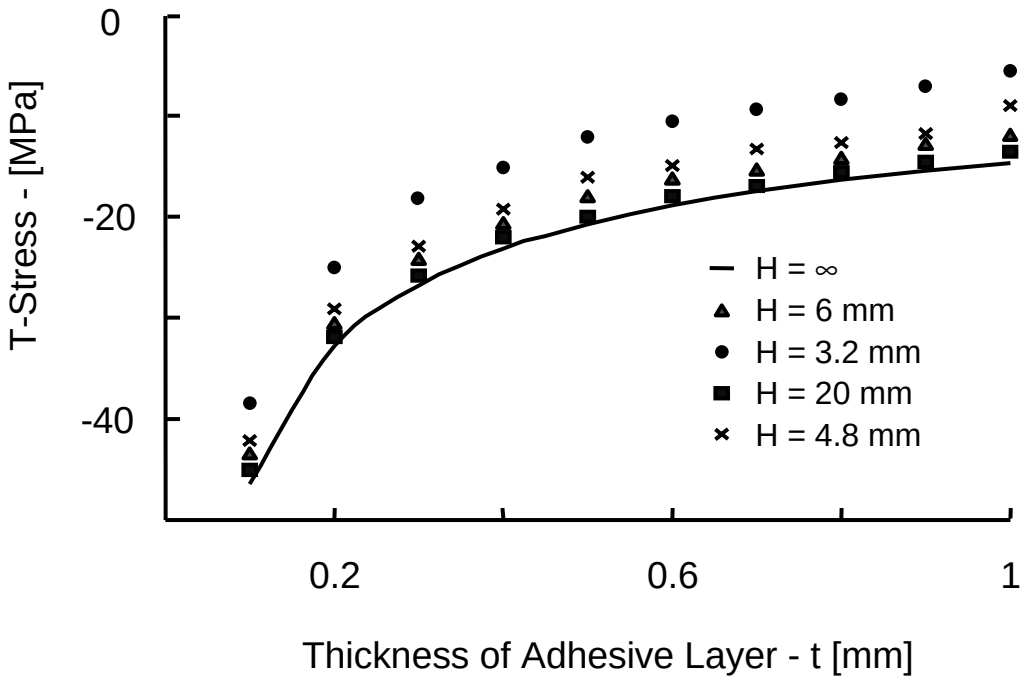

Fig. 9. The specimen geometry dependence of the T-stress in DCB specimens for specimens with no residual stress. Solid line represents Fleck, Hutchinson, and Suo [1] solution for semi-infinite adherends.

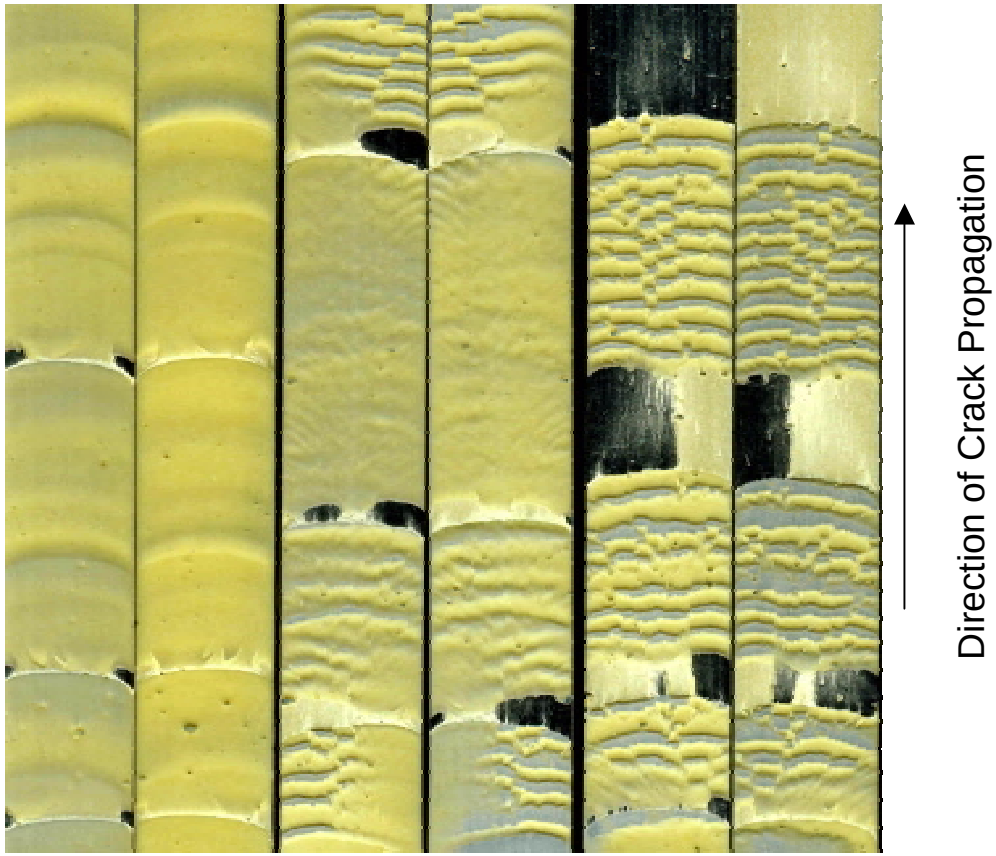

Fig. 10. The observed fracture surfaces in DCB specimens with different levels of plastic deformation. From left to right, the failures are cohesive with directionally stable crack, cohesive with oscillatory crack trajectory, and interfacial (or very close to the interface) with alternating crack trajectory.

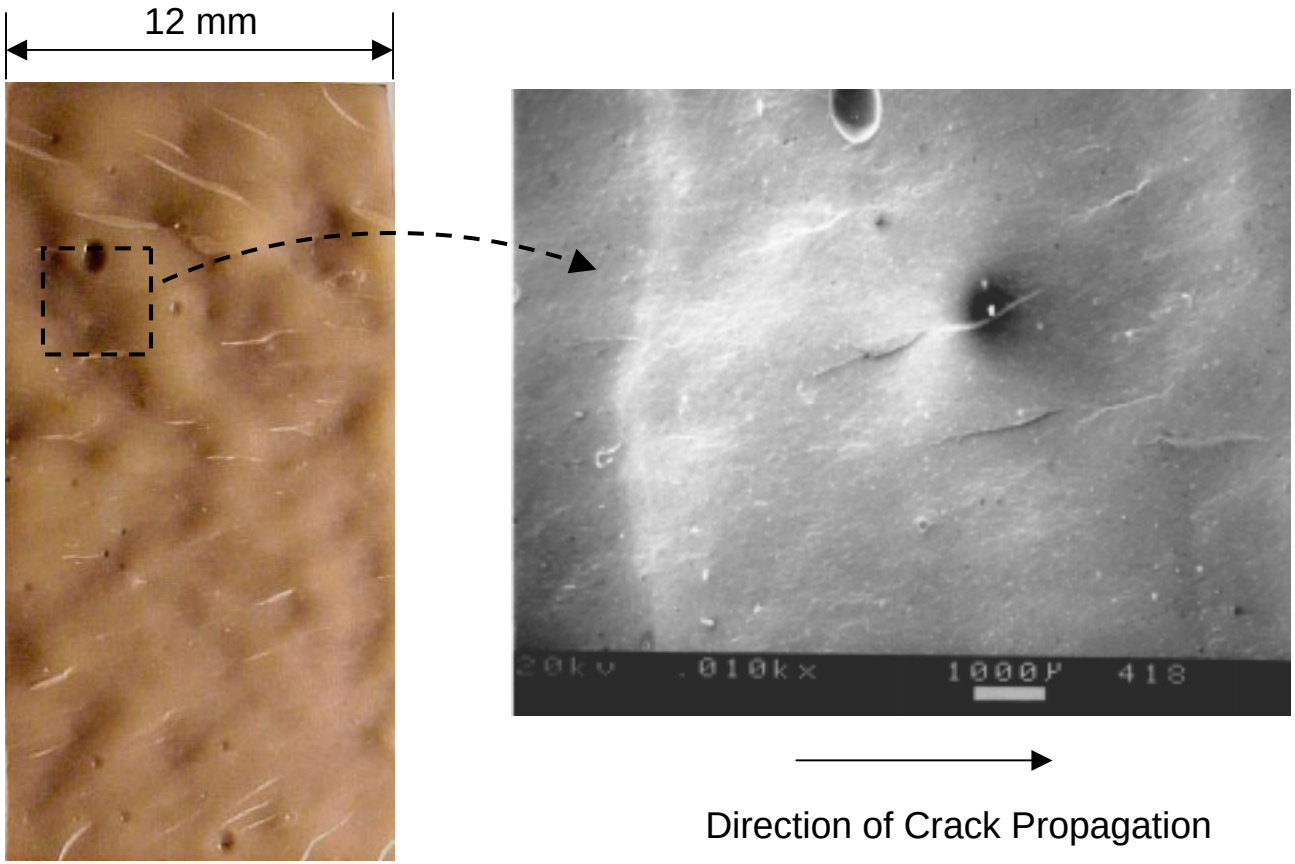

Fig. 11. Details of the failure surfaces of the DCB specimen with T = 29 MPa, in which oscillatory crack propagation was observed. The adhesive thickness of the specimen is 0.5 mm.

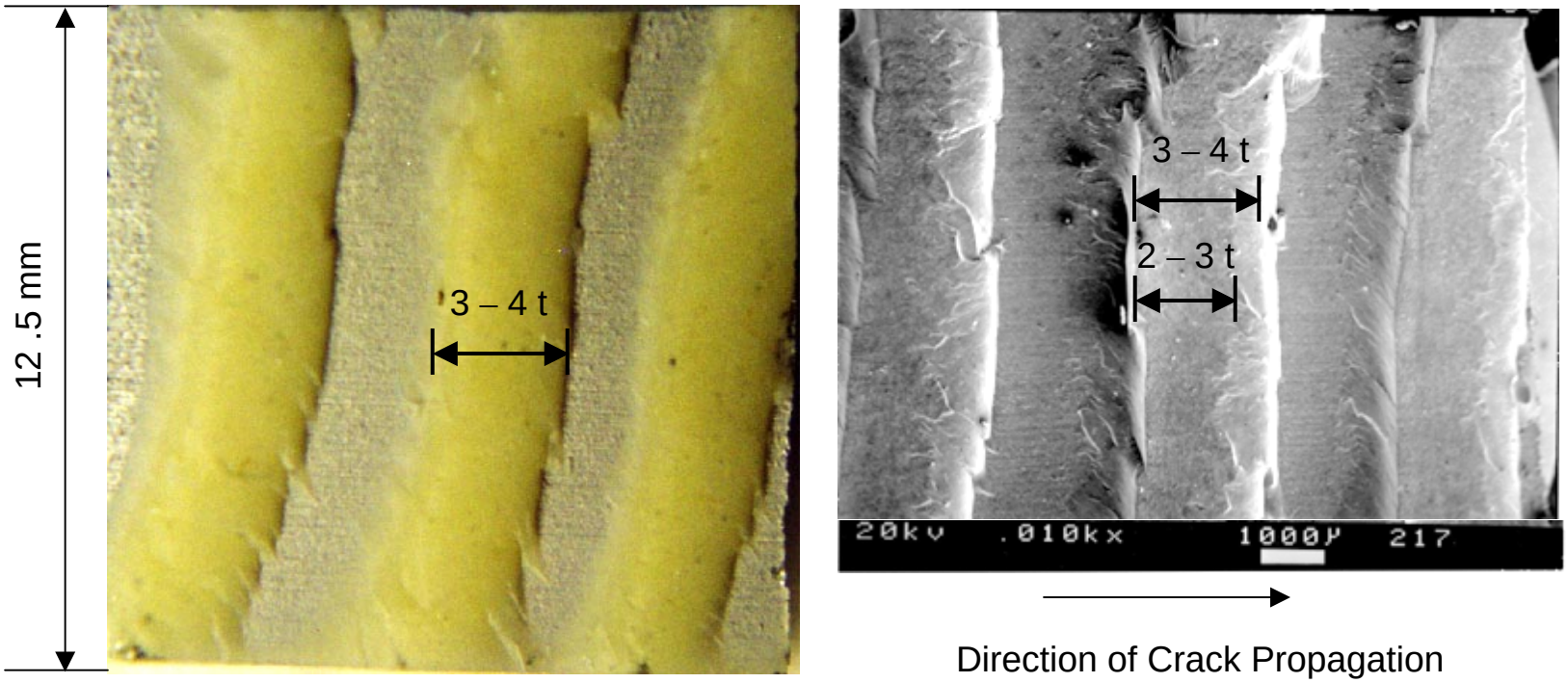

Fig. 12. Details of the failure surfaces of the specimen with T = 35 MPa, in which alternating crack propagation was observed. The adhesive thickness of the specimen is 0.5 mm.

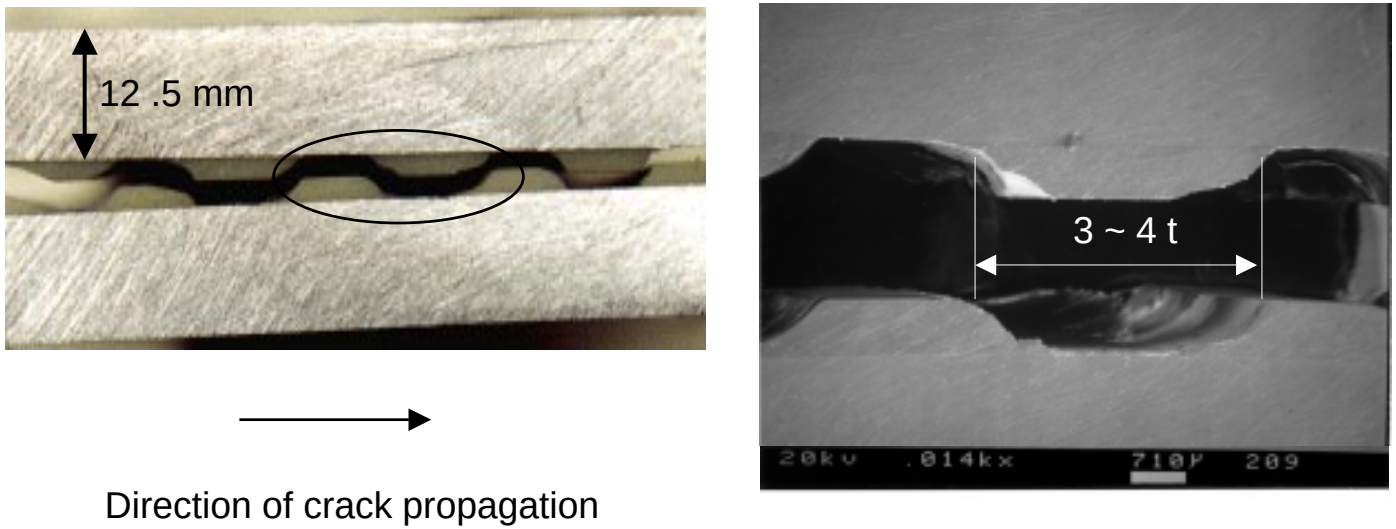

Fig. 13. The cross-section of the specimen with T = 35 MPa and alternating crack trajectory. The picture on the right is the scanning electron microscopy (SEM) micrograph of the circled portion of the cross-section. The adhesive thickness of the specimen is 0.5 mm.

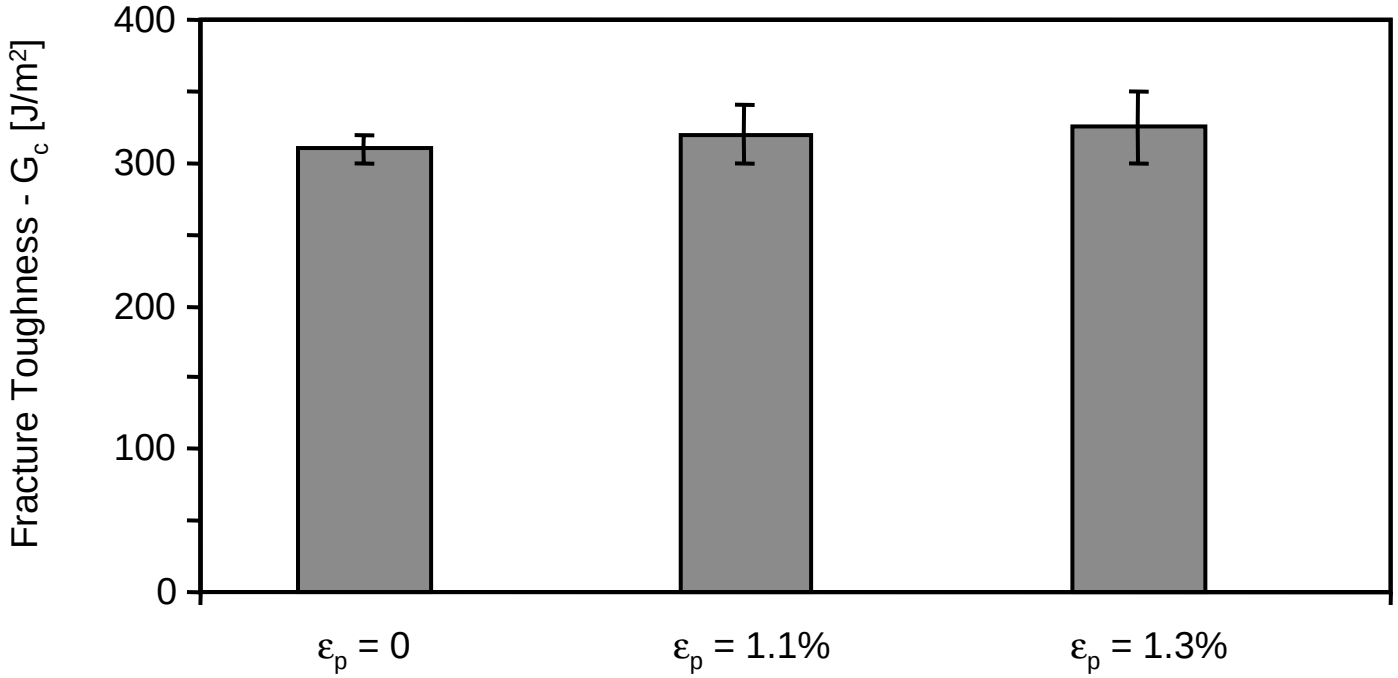

Fig. 14. The measured fracture toughness of the DCB specimens with different levels of plastic deformation. Error bars represent ± 1 standard deviation.

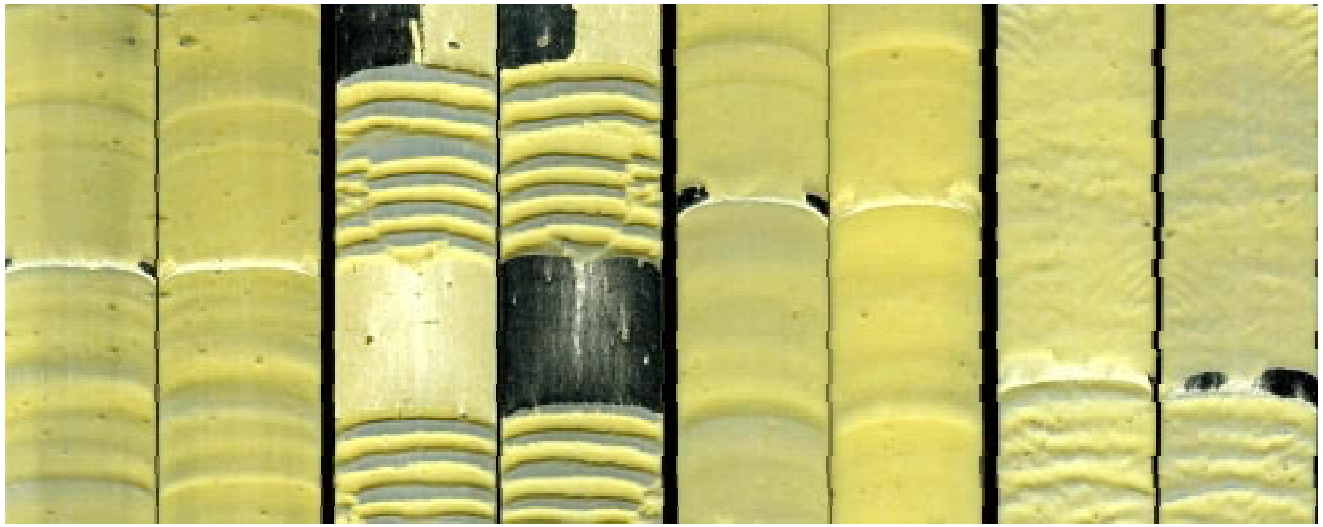

Fig. 15. The effect of adherend thickness on the T-stress level and the directional stability of cracks. The crack tends to be more directionally unstable when the thickness of adherend decreases.